Machining Science and Technology

ISSN: 1091-0344 (Print) 1532-2483 (Online) Journal homepage: http://www.tandfonline.com/loi/lmst20

MODELING OF 5-AXIS MILLING PROCESSES

E. Ozturk & E. Budak

To cite this article: E. Ozturk & E. Budak (2007) MODELING OF 5-AXIS MILLING PROCESSES, Machining Science and Technology, 11:3, 287-311

To link to this article: http://dx.doi.org/10.1080/10910340701554808

Published online: 02 Oct 2007.

Machining Science and Technology, 11:287–311

ISSN: 1091-0344 print/1532-2483 online
DOI: 10.1080/10910340701554808

Taylor & Francis
Taylor & Francis Group

MODELING OF 5-AXIS MILLING PROCESSES

E. Ozturk and E. Budak □ *Faculty of Engineering and Natural Sciences, Sabanci University, Istanbul, Turkey*

□ *5-axis milling operations are common in several industries such as aerospace, automotive and die/mold for machining of sculptured surfaces. In these operations, productivity, dimensional tolerance integrity and surface quality are of utmost importance. Part and tool deflections under high cutting forces may result in unacceptable part quality whereas using conservative cutting parameters results in decreased material removal rate. Process models can be used to determine the proper or optimal milling parameters for required quality with higher productivity. The majority of the existing milling models are for 3-axis operations, even the ones for ball-end mills. In this article, a complete geometry and force model are presented for 5-axis milling operations using ball-end mills. The effect of lead and tilt angles on the process geometry, cutter and workpiece engagement limits, scallop height, and milling forces are analyzed in detail. In addition, tool deflections and form errors are also formulated for 5-axis ball-end milling. The use of the model for selection of the process parameters such as lead and tilt angles that result in minimum cutting forces are also demonstrated. The model predictions for cutting forces and tool deflections are compared and verified by experimental results.*

Keywords 5-axis milling, Ball-end milling, Milling force

INTRODUCTION

5-axis milling is used extensively in the manufacturing of free form surfaces such as turbine engine components, dies and molds. In most of these cases, the manufacturing tolerances are very tight due to the required high quality and dimensional integrity. Tool and part deflections are important contributors to the dimensional errors; however, they can be predicted and kept under control by modeling cutting forces. In 5-axis milling, there are two additional cutting parameters compared to the 3 axis milling; namely lead and tilt angles. Selecting the optimum combination of lead and tilt angles is one of the most challenging parts of 5-axis ball-end milling. Generally, in the industry lead and tilt angles are selected based on

Address correspondence to E. Budak, Faculty of Engineering and Natural Sciences, Istanbul, Turkey. E-mail: ebudak@sabanciuniv.edu

experience or by trial and error. Modeling the effect of lead and tilt angles on the process can turn this challenge into an opportunity if the optimal values can be predicted. For a given 5-axis milling process, cutting forces and tool deflections can be simulated throughout the process. This way, if needed the process is modified to satisfy both the required quality and productivity. Hence, the 5-axis ball-end milling model presented in this article can be useful both in the selection of the cutting parameters and process simulation.

There have been numerous efforts for modeling of the ball-end milling processes. These can be grouped into three categories according to how material data is obtained, varying from completely analytical (Shatla and Altan, 2000; Fontaine et al., 2006) to completely experimental (Lazoglu, 2003; Gradisek et al., 2004; Ozturk et al., 2006). One analytical approach is to use the flow stress and thermal properties of the workpiece material to predict cutting forces in 3-axis ball-end milling (Shatla and Altan, 2000). Similarly, in the so-called thermo-mechanical modeling, the cutting behavior of work material is described by a model such as the Johnson–Cook law that considers thermal and strain rate effects on the flow stress. This is the approach used by Fontaine et al. (2006) to predict cutting forces in 3-axis ball-end milling. Mechanistic modeling is an experimental approach where the cutting force coefficients are calibrated for a given milling tool and workpiece pair at different axial depth of cuts. Gradisek et al. (2004), Lazoglu (2003), and Ozturk et al. (2006) are some of the authors who employed mechanistic method to predict ball-end milling forces in 3-axis milling. Budak et al. (1996) presented a hybrid method named as *mechanics of milling* for milling force modeling based on the orthogonal cutting data and the oblique cutting model. The *mechanics of milling* approach was employed by several authors in 3-axis ball-end milling (Yang and Park, 1991; Tai and Fuh, 1995; Lee and Altintas, 1996; Yucesan and Altintas, 1996; Engin and Altintas, 2001; Sadeghi et al., 2003).

Although there have been several works on the modeling of 3-axis ball-end milling processes, these have been very limited for 5-axis milling operations. Due to the lead and tilt angles, the determination of the engagement boundaries is more complicated in 5-axis milling, and has been mainly done using non-analytical methods. Larue and Altintas (2005) used ACIS solid modeling environment to determine engagement between the milling tool and the workpiece for flank milling. Clayton et al. (2000) proposed a mechanistic force model for 5-axis milling using a discretized cutting edge model to determine the engagement zone.

In another mechanistic 5-axis model, Zhu et al. (2001) modeled the cutting edge profile, and determined the engaged cut geometry by classification of the cutting point positions with respect to the workpiece surface. Later, Fussell et al. (2003) used discrete geometric models of the tool and

workpiece to determine the contact area, and simulated 5-axis ball-end milling forces mechanistically. In another study, Kim et al. (2003) predicted the cutting forces in 3-axis ball-end milling by using Z-mapping, and estimated the form errors by modeling the milling tool as a cantilever beam. In the previous works on 5-axis ball-end milling, the effects of lead and tilt angle on the process geometry and mechanics, and the surface finish have not been shown explicitly. Also, the form errors for 5-axis milling have not been formulated and presented before.

In this article, the cutting forces in 5-axis milling are modeled by using the *mechanics of milling* approach. This method needs orthogonal cutting data for a given work material. However, once this data is obtained, it can be applied to different machining processes and cutting tools, unlike mechanistic approach where the force coefficients have to be calibrated for each material and milling tool pair. This is especially critical for ball-end mills where cutting speed continuously varies along the cutting edges which is why the calibration tests are repeated for different axial depth of cut values in the mechanistic models (Lazoglu, 2003; Gradisek et al., 2004; Ozturk et al., 2006).

Furthermore, the effects of lead and tilt angles on the engagement limits between the milling tool and the workpiece are formulated in detail, and the scallop height which is an important parameter for surface quality, is calculated analytically. The milling forces in different modes of 5-axis milling are investigated and model predictions are verified. The use of the model in selection of the lead and tilt angles is also shown. After the cutting forces are predicted, tool deflections can be determined as well. For this, the predicted cutting forces are applied on the tool structure which is modeled as a beam, and the tool deflections in 5-axis milling are calculated. Therefore, this work presents an analytical model for the 5-axis milling geometry and the process, and can be used in the simulation and the optimization of the complex machining applications.

Henceforth, the paper is organized as follows: The geometry of ball-end mill and the 5-axis milling geometry are presented, the effects of the lead and tilt angles on the uncut chip thickness, the engagement boundaries and the scallop height are also shown. Then, force model is presented and the tool deflection formulation is given. Finally, the simulation and experiment results are presented and a summary of contributions is given.

GEOMETRY OF BALL-END MILL

Ball-end mills are mainly used in 3-axis and 5-axis milling. Since calculation of cutting forces requires determination of local cutting edge geometry, geometry of the ball-end mill is presented firstly. The detailed geometry of a ball-end mill is shown in Figure 1. A Cartesian tool

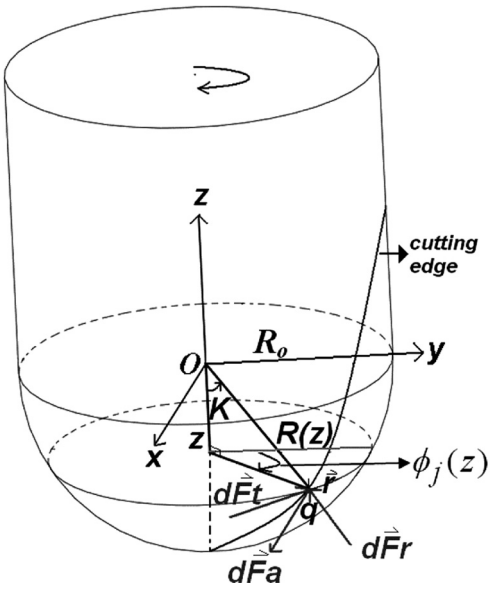

FIGURE 1 3D view of a ball-end mill.

coordinates system TCS (*xyz*) is defined at the ball center. The *z*-axis is the axial direction of the cutter. At the tool tip, the local radius *R(z)* is zero, and it increases along the *z*-axis in the ball part whereas it has a constant value of R_o in the cylindrical part:

$$\left.\begin{array}{ll} R(z) = \sqrt{R_o^2 - z^2} & \text{for ball part} \\ R(z) = R_o & \text{for cylindrical part} \end{array}\right\} \quad (1)$$

A point q on a cutting edge has local radius of *R(z)*, axial immersion angle of $K = K(z)$, and radial lag angle of $\psi(z)$ (Figure 2). The axial immersion angle K is defined as the angle between the tool axis and normal of the cutting edge at point q. The axial immersion angle K can be calculated as (Figure 1):

$$K = \sin^{-1}\left(\frac{R(z)}{R_o}\right) \quad (2)$$

The radial lag angle $\psi(z)$ is the angle on the *xy* plane between the line which connects the point q to the point (0, 0, z), and the cutting edge tangent at the tip of the cutter (Figure 2). Radial lag angle $\psi(z)$ is due to the helix angle and is calculated using Equation (3) (Lee and Altintas, 1996), where i_o is the helix angle at the meeting point of the ball and

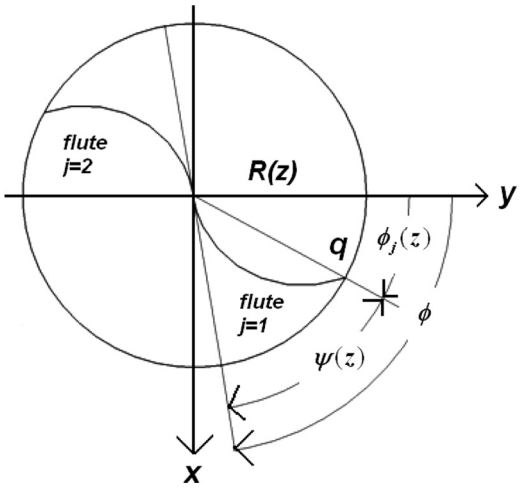

FIGURE 2 Top view of ball-end mill.

the cylinder parts.

$$\psi(z) = \frac{R_o + z}{R_o} \tan i_o \tag{3}$$

Immersion angle $\phi_j(z)$ shown in Figures 1 and 2 defines the angular orientation of a point on the cutting edge of flute j, measured from $+y$ direction whereas ϕ is the immersion angle of the reference tooth at the tool tip. $\phi_j(z)$ can be expressed as in Equation (4):

$$\phi_j(z) = \phi + (j-1)\phi_p - \psi(z) \tag{4}$$

where ϕ_p is the pitch angle between the preceding flutes. The pitch angle, ϕ_p, depends on the total number of teeth on the tool, n:

$$\phi_p = \frac{2\pi}{n} \tag{5}$$

5-AXIS MILLING GEOMETRY

The additional parameters in 5-axis milling, i.e., the lead and tilt angles, are defined in this section. Calculation of the uncut chip thickness and the engagement boundaries are presented. Scallop height h_s, which is a measure of surface property, are also formulated. In this model, two right-handed Cartesian coordinate systems are used (Figure 3). In a process coordinate system FCN and a tool coordinate system TCS (xyz). F is the feed

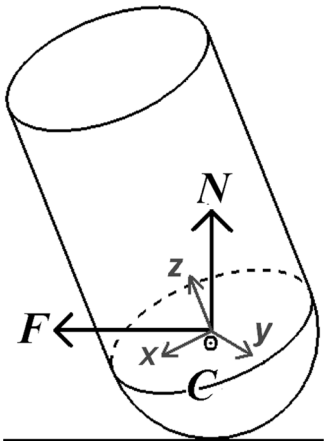

FIGURE 3 FCN and TCS (xyz) coordinate systems.

axis, C is the cross-feed axis and N is the surface normal axis of workpiece in FCN coordinate system. TCS is the rotated form of the FCN coordinate system and z axis is in the direction of the tool axis.

The lead angle is defined as the angular rotation of the milling tool axis about the cross-feed axis C, and the tilt angle is the rotation of the milling tool axis about the feed axis F as shown in Figure 4.

Since two coordinate systems are used in the model, a transformation between these coordinate systems is needed. Transformation matrix $\boldsymbol{T}$ is used to transform the coordinates, forces, and deflections from TCS to FCN:

$$\begin{bmatrix} F \\ C \\ N \end{bmatrix} = \boldsymbol{T} \begin{bmatrix} x \\ y \\ z \end{bmatrix} \tag{6}$$

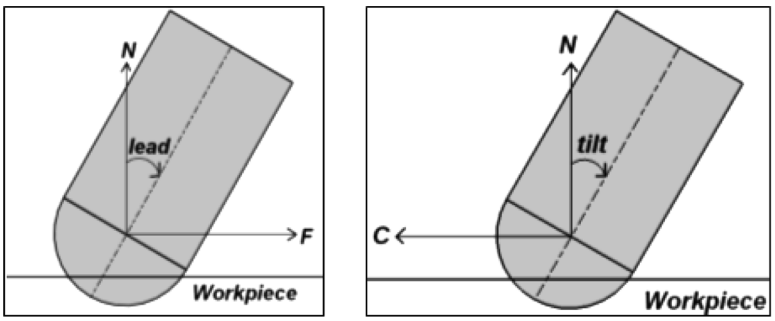

FIGURE 4 Lead and tilt angle representation.

$\boldsymbol{T}$ is the combination of two Euler transformations for lead and tilt angles, and it is calculated by Equation (7), where l and t represent the lead and tilt angles, respectively.

$$\boldsymbol{T} = \begin{bmatrix} 1 & 0 & 0 \\ 0 & \cos t & -\sin t \\ 0 & \sin t & \cos t \end{bmatrix} \begin{bmatrix} \cos l & 0 & \sin l \\ 0 & 1 & 0 \\ -\sin l & 0 & \cos l \end{bmatrix} \tag{7}$$

Uncut Chip Thickness

Uncut chip thickness is the thickness of the material removed instantaneously by the cutting edge in the normal direction. In ball-end milling, uncut chip thickness at a point on the cutting edge depends on the immersion angle ϕ and the z coordinate of the point. Then, the uncut chip thickness ct at a point on the cutting edge can be determined by the scalar product of the feed vector $\vec{t}$ and the unit outward surface normal vector $\vec{u}$ of the tool at the cutting point (see Figure 5):

$$ct = \vec{t} \cdot \vec{u} \tag{8}$$

The feed vector $\vec{t}$ and unit outward surface normal vector $\vec{u}$ are calculated in the FCN coordinate system. The feed vector $\vec{t}$ is defined as:

$$\vec{t} = f_t \vec{f} \tag{9}$$

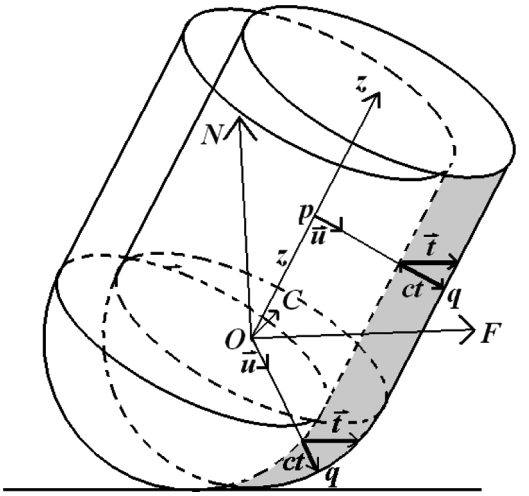

FIGURE 5 Uncut chip thickness *ct*.

In Equation (9), f_t is the feed per tooth and $\vec{f}$ is the unit vector in the feed direction F. Unit outward surface normal vector $\vec{u}$ calculation is different for the ball and the cylinder parts (see Figure 5). For the ball part, the surface normal vector $\vec{u}$ at a point q on the cutting edge can be calculated as:

$$\vec{u} = \frac{\vec{Oq}}{\left|\vec{Oq}\right|} = \frac{F\vec{f} + C\vec{c} + N\vec{n}}{R_o} \tag{10}$$

where F, C, N are the coordinates of the point q in FCN; and $\vec{c}$, $\vec{n}$ are the unit vectors in C axis and N axis, respectively. On the other hand, in the cylindrical part, the unit surface outward normal vector at a point q that is at elevation z is defined as follows:

$$\vec{u} = \frac{\vec{pq}}{\left|\vec{pq}\right|} \tag{11}$$

In the calculation of $\vec{pq}$ vector, first of all the point p is defined. The point p lies in the center of the ball-end mill in x, y axis in the TCS coordinate system and it has the same elevation with point q in z axis. Thus, the TCS coordinate of the point p is (0, 0, z). In order to define the $\vec{pq}$ vector in the FCN coordinates, the point p is transformed to the FCN system using the transformation matrix $\boldsymbol{T}$, and after defining (F_p, C_p, N_p) as the transformed coordinates of the point p in FCN coordinates, the $\vec{pq}$ vector is calculated as:

$$\vec{p}\,q = (F - F_p)\vec{f} + (C - C_p)\vec{c} + (N - N_p)\vec{n} \tag{12}$$

Another parameter used in the model is the chip width db that is tangent to cutting edge. It can be defined as follows:

$$db = \frac{dz}{\sin K} \tag{13}$$

Engagement Boundaries in 5-axis Ball-end Milling

In the engagement analysis, firstly coordinates of points on cutting edge on ball-end mill are determined in the TCS. Starting from tool tip, ball-end mill is divided into differential disc elements, having height of dz, along tool axis. For a disc element at a height of z, x and y coordinates of points on cutting edge are found in terms of local radius $R(z)$ and $\phi_j(z)$

which is calculated using Equation (4):

$$\begin{aligned} x &= R(z)\sin\phi_j(z) \\ y &= R(z)\cos\phi_j(z) \end{aligned} \tag{14}$$

However, engagement conditions are given in the FCN coordinate system. Thus, coordinates (x, y, z) of a point on the cutting edge need to be transformed from TCS to FCN using the transformation matrix $\boldsymbol{T}$ so as to check whether the corresponding point satisfies engagement conditions. The ones that satisfy the conditions are in cut with the workpiece. There are two different cases in the engagement analysis. In the first case, the tool cuts a non-machined cubic solid (first-cut, Figure 6a), whereas in the second case it cuts a previously machined surface (following-cut, Figure 6b).

The milling mode, i.e., up and down milling, definitions can be ambiguous for 5-axis ball-end milling. For example, the start and exit angles may not be 0 deg and 180 deg, respectively, due to the effect of lead and tilt angles. In order to define the direction of the uncut material, another parameter, cross-feed direction is used. If uncut material is in the positive C axis with respect to the milling tool, the cross-feed direction is positive. On the other hand, if uncut material is in the negative C axis with respect to the milling tool, the cross-feed direction is negative which is the case in Figure 6a and Figure 6b.

The common engagement conditions for both first-cut and following-cut cases are that chip thickness ct at the corresponding cutting point is greater than 0 and N coordinates of the points are equal to or less than $a - R_o$ (i.e., $N \leq a - R_o$) where a is the cutting depth. a is the distance between the tool's lowest point and workpiece's upper face in the surface normal direction N (Figure 6b, Figure 7a). In other words, it's the depth

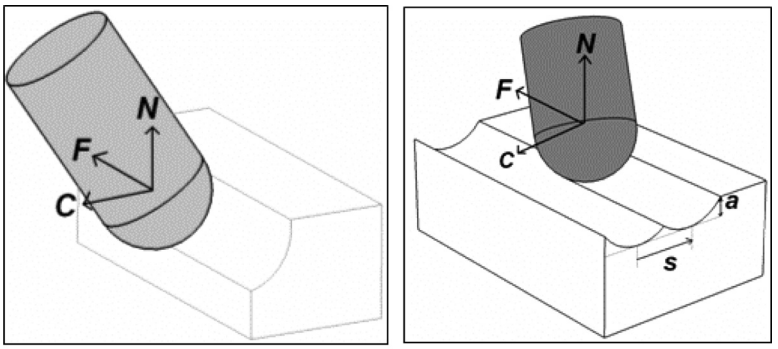

(a) (b)

FIGURE 6 Geometry of the (a) first-cut and (b) following cuts.

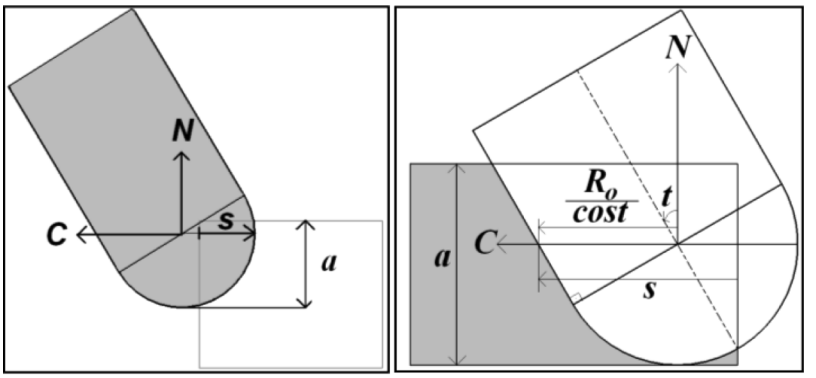

(a) (b)

FIGURE 7 (a) The step over s and the cutting depth a in the first-cut; (b) A first-cut process (cross feed direction positive, tilt angle negative).

of the stock removed in the surface normal direction N. It should be noted that the cutting depth is different than the axial depth which is along the tool axis in 5-axis ball-end milling due to the lead and tilt angles. The other engagement conditions, depending on whether process is first-cut or following-cut, are presented for the two cases separately.

In the first-cut case, step over s (Figure 7) is defined as the distance that the tool penetrates through the workpiece at the ball center level through C axis. Depending on the cross-feed direction and the tilt angle t, there are 4 different engagement conditions in C coordinates of points on the cutting edge for first cuts, which are tabulated in Table 1.

Engagement criteria determination for an example case where cross-feed direction is positive and tilt angle is negative is presented in Figure 7(b) for a first-cut process. In this case, the engagement condition in C coordinates is that the C coordinates of the points should be equal to or greater than $(R_o/\cos t) - s$.

In the following-cut cases, the step over s is the distance between the adjacent tool paths in C axis as shown in Figure 6(b). Depending on the cross-feed direction, step over s, tilt angle t, ball-end mill radius R_o and N coordinate of the point on the cutting edge; there are different engagement

TABLE 1 Engagement Criteria for the First-Cut Case

Case	Cross-feed direction	Tilt angle	Condition for engagement
1	Positive	$t \geq 0$	$C \geq R_o - s$
2		$t < 0$	$C \geq \frac{R_o}{\cos t} - s$
3	Negative	$t \geq 0$	$C \leq -\frac{R_o}{\cos t} + s$
4		$t < 0$	$C \leq -R_o + s$

TABLE 2 Engagement Conditions for the Following-Cut Case (Positive Cross-Feed Direction)

Case	Step over	Tilt angle	N coordinate	Condition for engagement
1	$s \le 2R_o \cos t$		$N \le -\sqrt{R_o^2 - \frac{s^2}{4}}$	–
2			$-\sqrt{R_o^2 - \frac{s^2}{4}} < N \le R_o \sin t$	$C \ge \sqrt{R_o^2 - N^2} - s$
3			$N > R_o \sin t$	$C \ge \frac{R_o - N \sin t}{\cos t} - s$
4	$s > 2R_o \cos t$	$t > 0$	$N \le N_s$	–
5			$N_s < N \le R_o \sin t$	$C \ge \sqrt{R_o^2 - N^2} - s$
6			$N > R_o \sin t$	$C \ge \frac{R_o - N \sin t}{\cos t} - s$
7		$t < 0$	$N \le N_s$	–
8			$N > N_s$	$C \ge \frac{R_o - N \sin t}{\cos t} - s$

conditions in C coordinate of the point. The engagement conditions for the following cut cases are tabulated in Tables 2 and 3 for the positive and negative cross-feed directions, respectively.

The engagement conditions given in Table 2 for the positive cross-feed direction case are explained here for the following-cuts. There are mainly 2 different geometric situations depending on the step over s. If s is less than $2R_o \cos t$, the ball part of the milling tool intersects with the ball part of the previous cut as shown in Figure 8a. In this case, there are three different engagement zones. In the first engagement zone, where the N coordinate of a cutting point on the cutting edge is below $N = -\sqrt{{R_o}^2 - s^2/4}$ plane, the point is in cut with the workpiece (case 1). The second engagement zone is bounded by the ball parts of the current and previous passes, $N = -\sqrt{{R_o}^2 - s^2/4}$ plane and $N = R_o \sin t$ plane. In this zone, the C coordinate of the cutting point should be equal to or higher than $\sqrt{{R_o}^2 - N^2} - s$ to be in cut (case 2). The last engagement zone is bounded by the cylinder parts of the current and previous passes, $N = R_o \sin t$ plane and $N = a - R_o$ plane. In this third zone, if the cutting point's C coordinate is equal to or higher than $(R_o - N \sin t/\cos t - s)$, the point is in cut with the workpiece (case 3).

In the other case, where step over is greater than $2R_o \cos t$, depending on the sign of the tilt angle there are 2 different conditions. However, a

TABLE 3 Engagement Conditions for the Following-Cut Case (Negative Cross-Feed Direction)

Case	Step over	tilt angle	N coordinate	Condition for engagement
1	$s \le 2R_o \cos t$		$N \le -\sqrt{R_o^2 - \frac{s^2}{4}}$	–
2			$-\sqrt{R_o^2 - \frac{s^2}{4}} < N \le -R_o \sin t$	$C \le -\sqrt{R_o^2 - N^2} + s$
3			$N > -R_o \sin t$	$C \le -\frac{R_o + N \sin t}{\cos t} + s$
4	$s > 2R_o \cos t$	$t > 0$	$N \le N_s$	–
5			$N > N_s$	$C \le -\frac{R_o + N \sin t}{\cos t} + s$
6		$t < 0$	$N \le N_s$	–
7			$N_s < N \le -R_o \sin t$	$C \le -\sqrt{R_o^2 - N^2} + s$
8			$N > -R_o \sin t$	$C \le -\frac{R_o + N \sin t}{\cos t} + s$

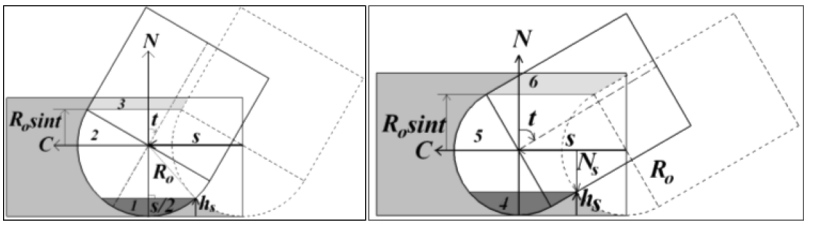

FIGURE 8 Cross-feed direction positive a) $s \leq 2R_o \cos t$ b) $s > 2R_o \cos t$, $t > 0$.

situation where tilt angle is positive is demonstrated in Figure 8b to be representative. In this case, the cylinder part of the milling tool intersects with the ball part of the previous pass at a point whose N coordinate is equal to N_s, where N_s is determined by equation 15 in terms of radius of ball-end mill R_o, the step over s and the tilt angle t:

$$N_s = -\sqrt{R_o{}^2 - (R_o - s\cos t)^2}\cos t - (R_o - s\cos t)\sin|t| \qquad (15)$$

For this case, there are three different engagement zones. In the first region where N coordinate of the cutting point is below $N = N_s$ plane, the point is in cut with the workpiece (case 4). The second region is bounded by the ball parts of the current and the previous passes, $N = N_s$ plane and $N = R_o \sin t$ plane (case 5). Engagement condition in this case is the same as case 2. Finally, the third engagement zone is bounded by the cylinder parts of the current and the previous passes, $N = R_o \sin t$ plane and $N = a - R_o$ plane (case 6). In this case engagement condition is the same as case 3. On the other hand, if tilt angle is negative(case 7 and case 8 in Table 2), there are two different engagement zones, i.e. the first one is below the $N = N_s$ plane and the second one is above the $N = N_s$ plane. In the first zone, the cutting point is in cut with the workpiece. The second zone is bounded by the cylinder parts of the current and the previous passes, $N = N_s$ plane and $N = a - R_o$ plane. Engagement condition in this zone is the same as case 3.

Scallop Height

Scallop height h_s is a measure of surface quality for the following-cut cases. In 3-axis ball-end milling, it depends on the radius of ball-end mill R_o and step over s. However, in 5-axis ball-end milling the tilt angle may also affect the scallop height. If step over is less than $2R_o \cos t$, the ball part of the milling tool intersects with the ball part of the previous cut; thus, scallop height calculation is the same as the 3 axis ball-end milling (Figure 8a).

TABLE 4 Scallop Height Formulation in 5-Axis Ball-End Milling

Step over	Scallop height h_s
$s \leq 2R_o \cos t$	$R_o - \sqrt{R_o^2 - \frac{s^2}{4}}$
$s > 2R_o \cos t$	$R_o + N_s$

On the other hand, if the step over is higher than $2R_o \cos t$, the cylindrical and the ball parts intersect as shown in Figure 8b, and scallop height also depends on tilt angle. Scallop height formulations are given in Table 4 for both of the cases.

In the following-cuts, the step over can be as high as $2R_o/\cos t$. In this case the maximum scallop height is $h_{s,\max} = R_o(1 + \sin|t|)$ provided that the cutting depth is sufficiently high. In order to show the effect of the step over on the scallop height, a normalized form of scallop height is used. The normalized scallop height is the ratio of the scallop height to the radius of the ball-end mill whereas normalized step over is the ratio of the step over to the maximum possible step over, i.e., $2R_o/\cos t$. As a representative case, for a fixed tilt angle of 60 deg, the variation of the normalized scallop height with the normalized step over is presented in Figure 9. In 3-axis ball-end milling, the maximum scallop height is equal to the radius of the ball-end mill. However, in 5-axis milling, the scallop height can be higher than the radius of the ball-end mill depending on the tilt angle and the step over as presented in Figure 9.

FORCE MODEL

Magnitude of cutting forces is an important limitation in a 5-axis milling process. If cutting forces reach high values, resulting deflections may cause unacceptably high form errors. Furthermore, high cutting forces may cause milling tool breakage due to excessive bending stresses as well as spindle overload. Thus, predicting cutting forces in 5-axis ball-end milling operations is important for selection of machining conditions.

In order to model cutting forces, the ball-end mill is divided into differential cutting elements where oblique cutting mechanics is used to

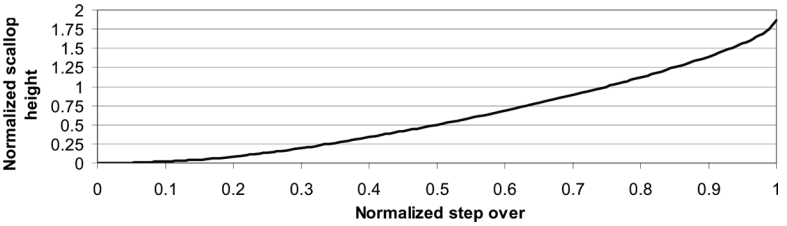

FIGURE 9 Normalized scallop height analysis.

determine differential forces. Cutting force and edge force coefficients are determined using the *mechanics of milling* method (Budak et al., 1996). In this approach, parameters (shear angle, friction angle and the shear stress) required for the calculation of cutting force coefficients are obtained from an orthogonal cutting database. The force model integrates the contribution of the differential cutting elements that are engaged with the workpiece for each rotational position of the tool, and calculates the cutting forces in TCS, and FCN coordinate systems.

The orthogonal databases are generated for different rake angles, feed rates and cutting speeds for a work-cutting tool material pair (Budak et al., 1996). In ball-end mills, in addition to the cutting speed and uncut chip thickness, radial, or velocity rake angle (Armarego and Brown, 1969) may also vary along the cutting edge depending on the path and the wheel profile used during the grinding of the flutes. Thus, together with the local cutting speed and uncut chip thickness value, corresponding normal rake angle must also be determined, and used in the calculation of the local cutting force coefficients. For the tools used in this study, the radial rake angle variation can be modeled as a sinusoidal one along the tool axis as follows:

$$\alpha_v = \begin{cases} \alpha_{vo} \sin K & -R_o < z < 0 \\ \alpha_{vo} & z \geq 0 \end{cases} \tag{16}$$

where α_{vo} is the radial rake angle at the ball-cylinder meeting boundary, and K is axial immersion angle given by Equation (2). Corresponding local normal rake angle, α_n, can be determined from the geometric relationship between two rake angles (Armarego and Brown, 1969).

$$\tan \alpha_n = \tan \alpha_v \cos i \tag{17}$$

where i is the inclination, or the local helix angle.

Cutting forces are separated into edge and shear cutting components in the linear edge force model. The cutting force coefficients, K_{rc}, K_{tc}, K_{ac}, and the edge force coefficients, K_{re}, K_{te}, K_{ae}, in radial, tangential and axial directions, respectively, are determined using the orthogonal database and the oblique cutting model (Budak et al., 1996). Thus, the differential cutting forces for the tooth j in the radial, tangential and axial directions at a point on the cutting edge can be determined as (Lee and Altintas, 1996):

$$\begin{aligned} \mathrm{d}F_{rj}(\phi_j(z)) &= K_{re}\,dS + K_{rc}(ct)\,db \\ \mathrm{d}F_{tj}(\phi_j(z)) &= K_{te}\,dS + K_{tc}(ct)\,db \\ \mathrm{d}F_{aj}(\phi_j(z)) &= K_{ae}\,dS + K_{ac}(ct)\,db \end{aligned} \tag{18}$$

In Equation (18), dS is the differential cutting edge length (Lee and Altintas, 1996). The differential forces in radial, tangential and axial directions can be transformed into the tool coordinate system TCS as follows (Lee and Altintas, 1996):

$$\begin{bmatrix} dF_{xj}(\phi_j(z)) \\ dF_{yj}(\phi_j(z)) \\ dF_{zj}(\phi_j(z)) \end{bmatrix} = \boldsymbol{T}_{xyz} \begin{bmatrix} dF_{rj}(\phi_j(z)) \\ dF_{tj}(\phi_j(z)) \\ dF_{aj}(\phi_j(z)) \end{bmatrix} \tag{19}$$

where

$$\boldsymbol{T}_{xyz} = \begin{bmatrix} -\sin K \sin \phi_j(z) & -\cos \phi_j(z) & -\cos K \sin \phi_j(z) \\ -\sin K \cos \phi_j(z) & \sin \phi_j(z) & -\cos K \cos \phi_j(z) \\ \cos K & 0 & -\sin K \end{bmatrix} \tag{20}$$

The total cutting forces on the tool are calculated by integrating the differential forces acting on the oblique elements engaged with the workpiece for each immersion angle, and summing up the contribution of each cutting flute as follows:

$$\begin{aligned} F_x(\phi) &= \sum_{j=1}^{n} \int dF_{xj}(\phi_j(z)) \\ F_y(\phi) &= \sum_{j=1}^{n} \int dF_{yj}(\phi_j(z)) \\ F_z(\phi) &= \sum_{j=1}^{n} \int dF_{zj}(\phi_j(z)) \end{aligned} \tag{21}$$

Cutting forces can also be transformed to FCN using the transformation matrix $\boldsymbol{T}$:

$$\begin{bmatrix} F_F(\phi) \\ F_C(\phi) \\ F_N(\phi) \end{bmatrix} = \boldsymbol{T} \begin{bmatrix} F_x(\phi) \\ F_y(\phi) \\ F_z(\phi) \end{bmatrix} \tag{22}$$

FORM ERROR MODEL

Form error is a measure of dimensional part quality that is usually maintained using conservative cutting parameters such as low feed rates and depth of cuts, or by compensation. The former approach results in decreased productivity whereas the latter one may result in several scrap parts and time-consuming tests until the right offsets are identified. If form error is modeled for a cutting process before machining, the part can be machined correctly at the first try by offsetting the tool path based on the form errors predicted. This is the motivation behind the modeling of form errors.

For form error prediction, the predicted cutting forces are used together with the tool and workpiece structural models in order to determine the deflections. The form error is the relative deflection between the tool and the workpiece at a surface generation point. In this article, only the deflections of the milling tool are considered for simplicity, however part deflections can also be determined through the Finite Element Analysis (Budak and Altintas, 1994).

A ball-end mill can be modeled as a cantilever beam with elastic supports as shown in Figure 10. Cutting forces F_x, F_y and F_z on the tool when generating the cutter contact point *CC* are inserted into the beam deflection equations (Budak and Altintas, 1994) to find the deflections *in x*, *y* and *z* axes (δ_x, δ_y, δ_z). Since the tool is very rigid in z-axis with respect to *x* and *y* axis, deflection in the *z* direction can be neglected unless the part is flexible in *z* direction. Deflections in feed, cross-feed and surface normal axes (δ_F, δ_C, δ_N) are also calculated using transformation matrix $\boldsymbol{T}$ as in Equation (6).

CC point is defined as the tool's lowest point in surface normal axis *N* that is engaged with the workpiece. In first-cut cases, *CC* point coordinates in the FCN coordinate system depend on step over *s*, cross-feed direction and tilt angle. There are 8 different cases in *CC* point calculation and coordinates of the *CC* point in FCN are tabulated for the first-cut cases in Table 5.

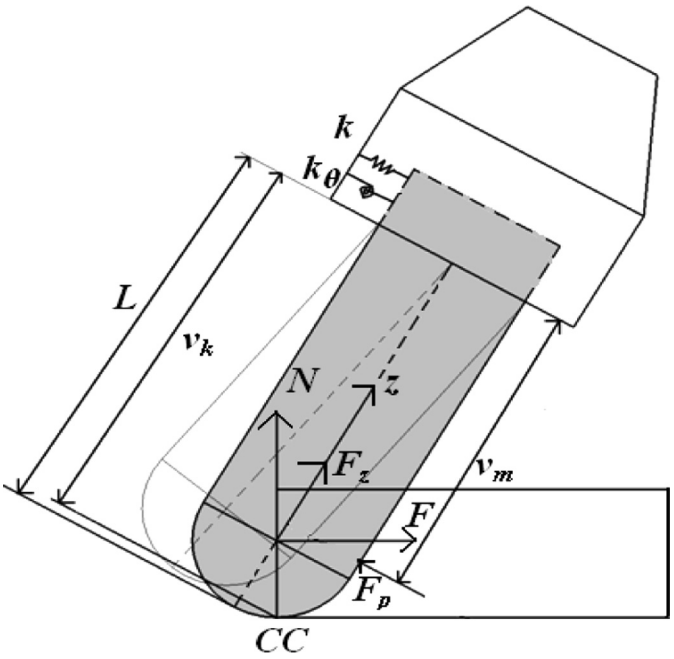

FIGURE 10 Structural model of the ball-end mill.

TABLE 5 Coordinates of the *CC* Point for the First Cut Case in FCN Coordinate System

Case	Cross-feed direction	s	*CC point in FCN*
$1t \geq 0$	Positive	$s \geq R_o$	$[0, 0, -R_o]^T$
		$s < R_o$	$[0, R_o - s, -\sqrt{R_o^2 - (R_o - s)^2}]^T$
$2t < 0$	Positive	$s \geq \frac{R_o}{\cos t}$	$[0, 0, -R_o]^T$
		$\frac{R_o \sin^2 t}{\cos t} \leq s < \frac{R_o}{\cos t}$	$[0, \frac{R_o}{\cos t} - s, -\sqrt{R_o^2 - (\frac{R_o}{\cos t} - s)^2}]^T$
$3t \geq 0$	Negative	$s \geqslant \frac{R_o}{\cos t}$	$[0, 0, -R_o]^T$
		$\frac{R_o \sin^2 t}{\cos t} \leq s < \frac{R_o}{\cos t}$	$[0, -\frac{R_o}{\cos t} + s, -\sqrt{R_o^2 - (-\frac{R_o}{\cos t} + s)^2}]^T$
$4t \leq 0$	Negative	$s \geq R_o$	$[0, 0, -R_o]^T$
		$s < R_o$	$[0, -R_o + s, -\sqrt{R_o^2 - (-{R_o}^2 + s)^2}]^T$

On the other hand, in the following-cut cases the coordinates of the *CC* point are $[0, 0, -R_o]$.

EXPERIMENTAL RESULTS AND SIMULATIONS

Milling Force Predictions

In order to verify the model, 5-axis ball-end milling tests on Ti6Al4V material were performed at a 5-axis machining center. 12 mm diameter ball-end mills clamped by a shrink fit tool holder were used in the tests. A Kistler table type dynamometer (Type 9257BA) was used together with the signal conditioner (Type 5233A1) to measure cutting forces. Cutting force signals are low pass filtered at 200 Hz with an integrated low pass filter in signal conditioner.

To demonstrate the model's effectiveness in different cases, comparisons between simulated cutting forces and measured ones for one revolution of the milling tool are presented here for 9 different cases. However, totally 70 tests were carried out. 12 mm diameter carbide ball-end mills with 2 teeth, 8 deg. rake angle and helix angle of 30 deg. were used in the tests. The cutting conditions are given in Table 6. These cutting

TABLE 6 Cutting Parameters

Case	Lead, tilt (deg)	Step over (mm)	Cutting type	Cross feed direction	Cutting depth (mm)	Feed mm/tooth	n (rpm)
(a)	30, 30	Slotting	–	–	1.5	0.1	500
(b)	10, –15	Slotting	–	–	1.5	0.1	3000
(c)	15, 0	7.8	First cut	Positive	3	0.1	500
(d)	−15, 0	7.2	First cut	Positive	3	0.1	500
(e)	15, −15	7.8	First cut	Negative	3	0.1	500
(f)	15, 15	7	Following Cut	Positive	3	0.1	1000
(g)	15, 15	7.8	First cut	Positive	3	0.1	500
(h)	15, −15	7	Following Cut	Negative	3	0.1	500
(i)	15, 0	5.4	First cut	Positive	3	0.1	500

parameters are used in the 5-axis force model and the cutting forces are simulated for one revolution of the milling tool. The comparisons for 9 different cutting conditions are shown in Figure 11a–i. The full lines are the simulation results whereas dotted lines are the measured force values. Except the first case where the forces are plotted in the FCN coordinate system, in other cases forces are in the TCS (*xyz*).

Statistical Analysis of the Results

A statistical analysis was performed to compare the cutting force predictions with the measurements for 70 cutting tests. The prediction error was defined as the difference between the absolute maximum value

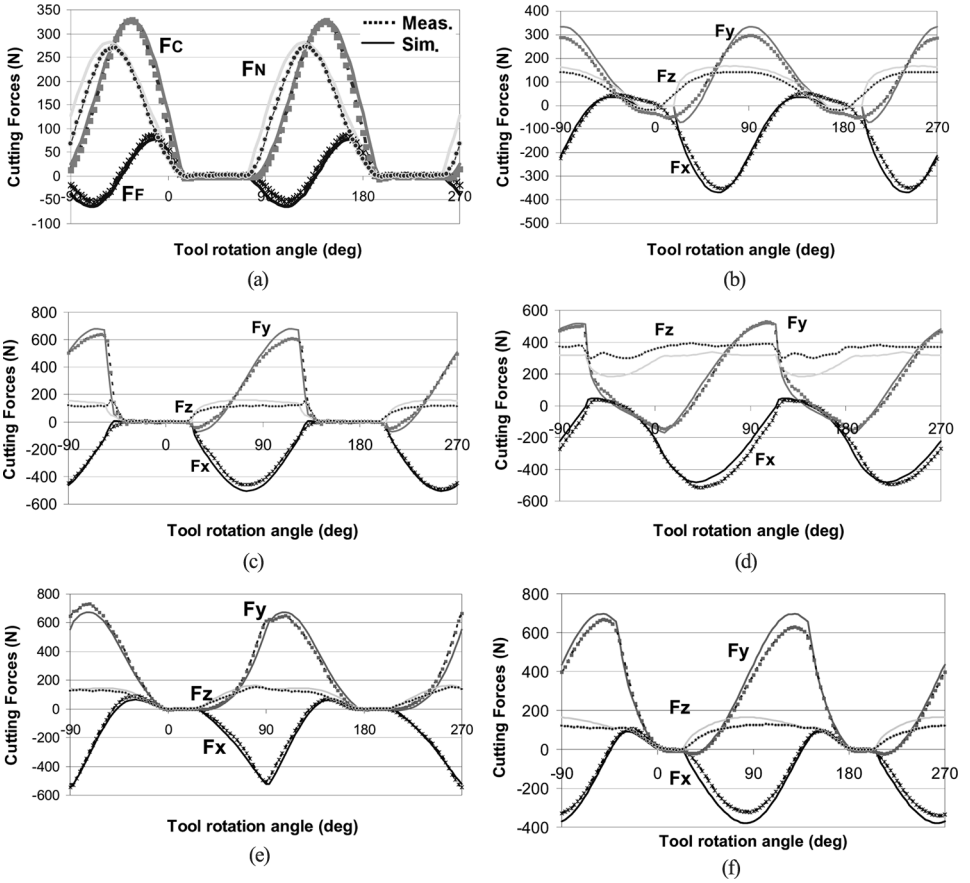

FIGURE 11 Comparison of measured and simulated cutting forces for cases (a)–(i), respectively.

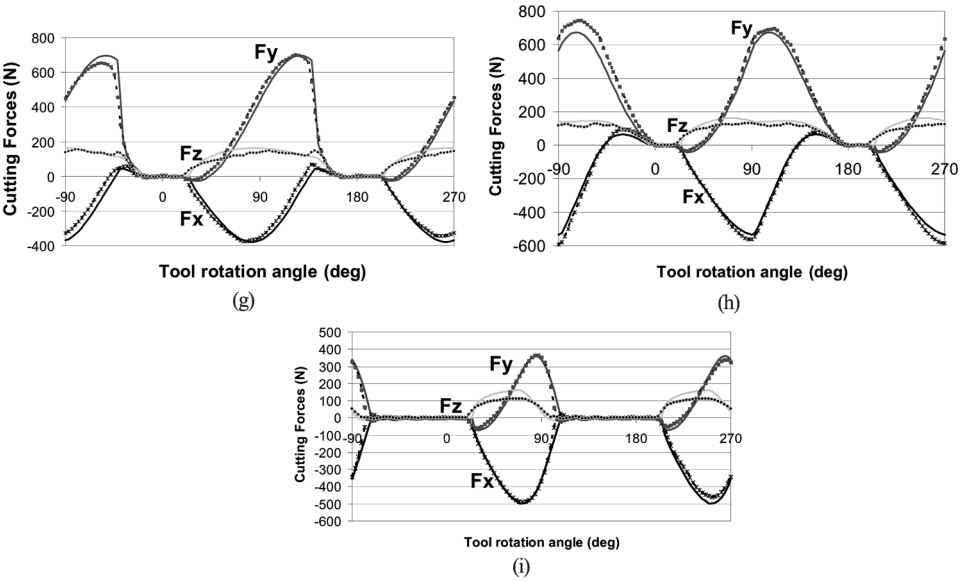

FIGURE 11. (Continued).

of measurement and absolute maximum value of prediction in percentage. The analysis was done for the forces in the TCS, i.e., F_x, F_y and F_z.

The distributions of prediction errors are shown for F_x, F_y and F_z in Figure 12. The mean of the prediction errors are 5%, 4% and −6% in F_x, F_y and F_z forces, respectively. The prediction accuracy for maximum force value in the x and y axis is in the 20% range. In some cases, it is observed that the prediction error in z direction may reach up to 50%. However, this is due to the fact that in these cases the F_z force is considerably lower in magnitude compared to F_x and F_y forces. An example of such a case is shown in Figure 11(i) where the maximum measured force in the z direction is 113 N, and the prediction for maximum F_z is 161 N.

Although there is an error of about 50%, the difference is only 48 N. It should be noted that the *mechanics of milling* method was used in the cutting force coefficient calculations, i.e., the orthogonal database generated for Ti4Al6V alloy by Budak et al. was directly used. Thus, the calibrations for the force coefficients were not performed for the milling tool used in the tests unlike the mechanistic method. Considering this, it can be claimed that the model predictions are reasonable. However, in cases where the lead angle is negative and the tool tip is cutting into the workpiece, which is the case shown in Figure 13, the simulations underestimate the cutting forces in the z direction, e.g., the case shown in Figure 11d. This is explained in the following section.

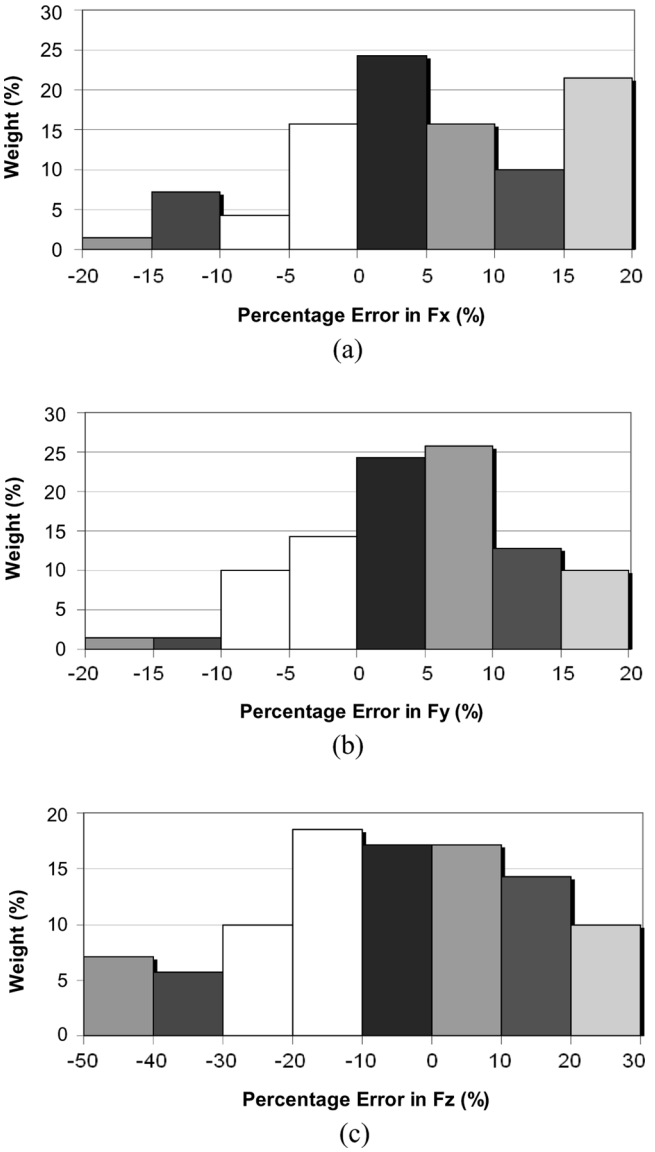

FIGURE 12 Statistical analysis for prediction error in (a) F_x (b) F_y (c) F_z.

The Effect of the Tool Tip Contact

When the lead angle is negative and the tool tip is cutting into the workpiece, the tip of the ball-end mill moves towards the workpiece since the feed vector has a nonzero component in the tool axis direction. Hence, the tool tip tries to penetrate into the workpiece. This phenomenon can not be modeled by the cutting mechanism since the cutting speed is zero

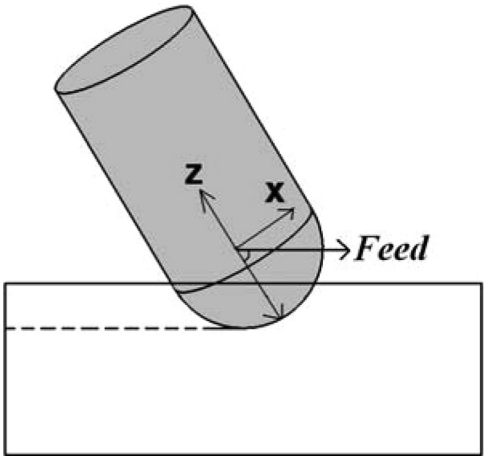

FIGURE 13 Indentation case.

at the tool tip. As a result of this contact between the tool tip and the workpiece, the tool faces an extra indentation force.

In order to show the effect of indentation force on the prediction accuracy, a separate statistical analysis was performed for the cases when tool tip is in cut with the workpiece. The result of this analysis is presented in Figure 14. The mean of the prediction error in F_z is 18% in these cases. The increase in the mean of the prediction error verifies the existence of indentation force for those cases. The indentation force can be modeled, or calibrated for more accurate predictions. However, it is well known that this tool orientation, i.e., negative tilt angle with tool tip in cut, is not a preferred mode of milling, and that's why this has not been taken as a priority for the force modeling.

Tool Deflection Predictions

Once the cutting forces are calculated, tool deflections can be predicted. Since the workpiece used in the tests is a rigid block, its deflections

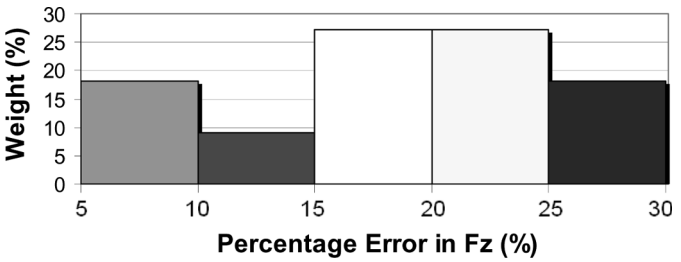

FIGURE 14 Statistical analysis for cases where the tilt angle is negative and the tool tip is in cut with workpiece.

TABLE 7 The Predicted and Measured Form Errors in the Surface Normal Direction

Case	δ_N (Simulation) mm	δ_N (Measurement)
g	0.045	0.040
h	0.017	0.014

were neglected. For two of the cases presented in Figures 11g and 11h, the errors in the surface normal direction δ_N were measured using a dial gauge and are compared with the model predictions in Table 7.

As can be seen from the above table, there is a good agreement between the measurements and the predictions for the form errors. The small difference can be attributed to the measurement errors, run-out of the tool, and the variation of the clamping stiffness k and k_θ during cutting.

Selection of Lead and Tilt Angles for Minimum Cutting Forces

The presented model can be used as an optimization tool while designing a new 5-axis ball-end milling process. The effect of the parameters such as feed rate and the depth of cut are usually predictable. On the other hand, the effects of the lead and the tilt angles on the process are not well known. Thus, the model can be used to determine the lead and tilt angles which will result in minimum milling forces. As an example, for a 5-axis ball-end milling process, the effects of the lead and the tilt angles are demonstrated next. A slotting case with 5 mm cutting depth,

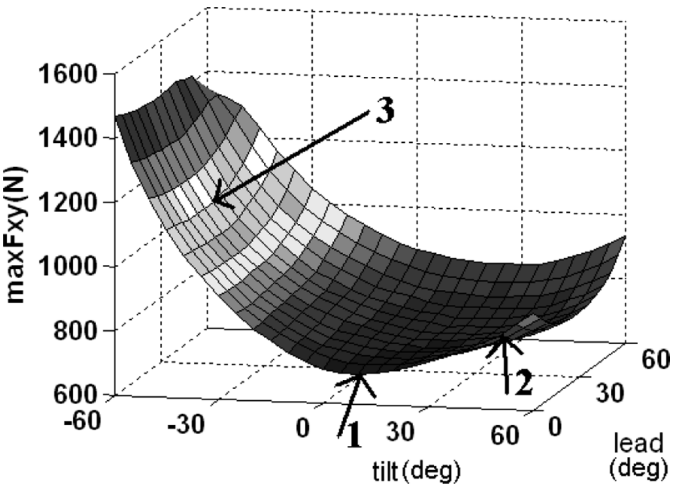

FIGURE 15 Maximum F_{xy} force in one revolution of the milling tool vs. lead and tilt angles.

TABLE 8 Simulation and Measurement Comparison for Sample Case

Point	lead, tilt deg.	Simulated maximum F_{xy}(N)	Measured maximum F_{xy}(N)
1	0, 10	692	653
2	0, 50	821	786
3	30, −50	1190	1110

and 0.05 mm/tooth feed rate is considered where the spindle speed is 1000 rpm. The milling tool is the same tool that was used in the previous tests, and the workpiece material is Ti6Al4V. In order to see the effects of the lead and the tilt angles on the forces, [0, 60] deg. range for the lead angle, and [−60, +60] deg. range for the tilt angle with 5 deg. increments were used in the simulations. The objective can be to determine the minimum of the cutting forces, tool deflection or surface error, power etc. In this sample analysis, the resultant force in the *xy* plane, F_{xy}, is selected to be minimized. Maximum F_{xy} force in one revolution of the milling tool is plotted as a function of the lead and the tilt angles in Figure 15.

From the figure, for this case one can conclude that the effect of the tilt angle on the F_{xy} is more than the effect of the lead angle, and the negative high tilt angles must be avoided. In addition, the minimum F_{xy} is obtained when the lead angle is 0 deg. and the tilt angle is 10 deg. (point 1 in Figure 15). In order to verify these predictions, cutting tests were performed for 3 points on the surface in Figure 15. The comparison between the predictions and the measurements is presented in Table 8. It can be concluded that the presented 5-axis milling force model can be used in the selection of the lead and tilt angle combination that will result in minimum cutting forces for given cutting conditions.

CONCLUSIONS

An analytical model is presented for 5-axis milling processes. The formulations for the geometry, engagement conditions, scallop height, cutting forces and tool deflections are given in detail by demonstrating the effects of lead and tilt angles. The simulated and measured milling forces and tool deflection errors are compared, and it is demonstrated that the model's predictions are reasonably accurate although no calibration for the force coefficients was performed for the milling tool used. It is also demonstrated that the indentation force that is observed when the lead angle is negative and tool tip is in cut, needs to be modeled or calibrated for increased accuracy.

The presented model can be used in industry, for process simulation and process optimization and it can be integrated into CAD/CAM programs. Cutting parameters of an existing 5-axis ball-end milling process

can be used in the model to simulate the cutting forces and form error in the process. If forces and deflections are higher than the acceptable limits, the process parameters can be modified using the model to improve productivity. Moreover, while designing a new 5-axis milling operation, the model can be embedded into an optimization algorithm to determine the optimum cutting parameters in the process.

ACKNOWLEDGEMENT

The authors acknowledge Scientific and Technical Research Council of Turkey (TUBITAK) for its support in this research.

NOMENCLATURE

TCS	right-handed tool coordinate system
FCN	right-handed process coordinate system
x, y, z	coordinates of points on cuttting edge in TCS
F, C, N	coordinates of points on cuttting edge in FCN
R_o	radius of ball-end mill
$R(z)$	local radius of ball-end mill
K	axial immersion angle
$\psi(z)$	local radial lag angle
i_o	helix angle at the meeting point of the ball and the cylinder parts
ϕ	immersion angle of the reference tooth at the tool tip, measured from $+y$ direction
$\phi_j(z)$	immersion angle that defines the angular orientation of a point on the cutting edge of flute j
ϕ_p	pitch angle
l	lead angle
t	tilt angle
ct	uncut chip thickness
$\vec{t}$	feed vector
$\vec{u}$	unit outward surface normal vector
f_t	feed per tooth
$\vec{f}, \vec{c}, \vec{n}$	unit vectors in F axis, C axis and N axis, respectively
db	chip width
dz	height of differential disc elements
a	cutting depth
s	step over
h_s	scallop height
α_{vo}	radial rake angle at the ball-cylinder meeting boundary

α_n	local normal rake angle
i	inclination or local helix angle
dS	differential cutting edge length
F_x, F_y, F_z	cutting forces in x, y, z axis, respectively
F_F, F_C, F_N	cutting forces in F, C, N axis, respectively
δ_x, δ_y, δ_z	deflections in x, y, z axis, respectively
δ_F, δ_C, δ_N	deflections in F, C, N axis, respectively

REFERENCES

Armarego, E.J.A.; Brown, R.H. (1969) *The Machining of Metals*, Prentice-Hall, Englewood Cliffs, NJ.

Budak, E.; Altintas, Y. (1994) Peripheral milling conditions for improved dimensional accuracy. *International Journal of Machine Tools and Manufacture*, 34(7): 907–918.

Budak, E.; Altintas, Y.; Armarego, E.J.A. (1996) Prediction of milling force coefficients from orthogonal cutting data. *Journal of Manufacturing Science and Engineering*, 118: 216–224.

Clayton, P.A.; El-Wardany, T.; Elbestawi, M.A.; Viens D. (2000) A mechanistic force model of the 5-axis milling process. *Proceedings of the ASME Manufacturing Engineering Division*, 11: 979–987.

Engin, S.; Altintas, Y. (2001) Mechanics and dynamics of general milling cutters part 1: helical end mills. *International Journal of Machine Tools and Manufacture*, 41: 917–924.

Fontaine, M.; Devillez, A.; Moufki, A.; Dudzinski, D. (2006) Predictive force model for ball-end milling and experimental validation with a wavelike form machining test. *International Journal of Machine Tools and Manufacture*, 46: 367–380.

Fussell, B.K.; Jerard, R.B.; Hemmet, J.G. (2003) Modeling of cutting geometry and forces for 5-axis sculptured surface machining. *Computer Aided Design*, 35: 333–346.

Gradisek, J.; Kalveram, M.; Weinert, K. (2004) Mechanistic identification of specific force coefficients for a general end mill. *International Journal of Machine Tools and Manufacture*, 44: 401–414.

Kim, G.M.; Kim, B.H.; Chu, C.N. (2003) Estimation of cutter deflection and form error in ball-end milling processes. *International Journal of Machine Tools and Manufacture*, 43: 917–924.

Larue, A.; Altintas, Y. (2005) Simulation of flank milling processes. *International Journal of Machine Tools and Manufacture*, 45: 549–559.

Lazoglu, I. (2003) Sculpture surface machining: a generalized model of ball-end milling force system. *International Journal of Machine Tools and Manufacture*, 43: 453–462.

Lee, P.; Altintas, Y. (1996) Prediction of ball-end milling forces from orthogonal cutting data. *International Journal of Machine Tools and Manufacture*, 36: 1059–1072.

Ozturk, B.; Lazoglu, I.; Erdim, H. (2006) Machining of free-form surfaces. part ii: calibration and forces. *International Journal of Machine Tools and Manufacture*, 46: 736–746.

Sadeghi, M.H.; Haghighat, H.; Elbestawi, M.A. (2003) A solid modeler based ball-end milling process simulation. *International Journal of Advanced Manufacturing Technology*, 22: 775–785.

Shatla, M.; Altan, T. (2000) Analytical modeling of drilling and ball-end milling. *Journal of Materials Processing Technology*, 98: 125–133.

Tai, C.; Fuh, K. (1995) The prediction of cutting forces in the ball-end milling process. *Journal of Materials Processing Technology*, 54: 286–301.

Yang, M.; Park, H. (1991) The prediction of cutting force in ball-end milling. *International Journal of Machine Tools and Manufacture*, 31(1): 45–54.

Yucesan, G.; Altintas, Y. (1996) Prediction of ball-end milling forces. *Journal of Engineering for Industry*, 118: 95–103.

Zhu, R.; Kapoor, S.G.; DeVor, R.E. (2001) Mechanistic modeling of the ball-end milling process for multi-axis machining of free-form surfaces. *Journal of Manufacturing Science and Engineering*, 123: 369–379.